

Quantifying Drift-Selection Balance Using an Agent-Based Biofilm Model of Identical Heterotrophs Under Low Nutrient Conditions

Joseph Earl Weaver*

4 School of Civil Engineering & Geosciences, Newcastle University, Cassie Building, Newcastle upon
5 Tyne, NE1 7RU, United Kingdom

⁶ * Corresponding author(s). E-mail: Joe.Weaver@newcastle.ac.uk

Abstract

Both deterministic and stochastic forces shape biofilm communities, but the balance between those forces is variable. Quantifying the balance is both desirable and challenging. For example, drift-driven drift failure, a stochastic force, can be thought of as an organism experiencing ‘bad luck’ and manipulating ‘luck’ as a factor in real world systems is difficult. We used an agent-based model to manipulate luck by controlling seed values governing random number generation. We determined which organism among identical competitors experienced the greatest drift-driven failure, gave it a deterministic growth advantage, and re-ran the simulation with the same seed. This enabled quantifying the growth advantage required to overcome drift, *e.g.*, a 50% chance to thrive may require a 10-20% improved growth rate. Further, we found that crowding intensity affected that balance. At moderate spacings, there were wide ranges where neither drift nor selection dominated. Those ranges shrank at extreme spacings; close and loose crowding respectively favoured drift and selection. We explain how these results may partially illuminate two conundrums: the fact that a stably operating wastewater treatment plant’s

24 microbial community can vary greatly over time and the difference between
25 equivalent and total community size in neutral community assembly models.

26 **Keywords:** agent-based model, biofilm, drift, neutral assembly, community
27 assembly, individual based model

28 1 Introduction

29 Both stochastic and deterministic assembly processes can shape biofilm communiti^{es}.^{1,2} Those
30 processes, however, rarely act equally and the balance between them is determined by many
31 conditions related to competition intensity. Such conditions include population size,^{3,4} available
32 space,⁵ and resource availability.⁶ Understanding how this balance shifts under differing conditions
33 provides insights into biofilm-associated systems such as environmental bioreactors, healthcare,
34 industrial production, and natural ecosystems.

35 Here, we attempt to quantify the balance between drift, a pure stochastic process,^{1,3} and a more
36 deterministic kinetic advantage. Under this balance, even if losing the ‘drift lottery,’ an individual’s
37 progeny may thrive if their maximum growth rate (μ_{max}) or half saturation constant (K_s) confers a
38 selection advantage over their competitors.

39 Such quantification is challenging. Drift is an inherently random process and experimental
40 manipulation of a random process, distinct from simply controlling for it, is difficult. Despite that
41 difficulty, there have been some physical experiments in which drift is isolated as an experimental
42 factor,^{4,7,8} often requiring subtle statistical analyses or extremely precise experimental work.

43 An alternative approach, used here, is to perform the experiments *in silico* where drift may be
44 directly manipulated via random number generation. We used an agent-based model (NUFEB)^{9,10} to
45 simulate spatially competing bacteria under low nutrient conditions. The bacteria were identical and
46 evenly spaced, differentiated only by random growth directions and biomass allocations during
47 division. Drift was therefore the only selection process and was controlled by the seed value
48 initializing the random number generator.

49 Our goal was to determine the degree to which a deterministic factor (here, Monod kinetics) must
50 improve to overcome drift-driven failure so subsequent simulations using identical seeds were run.
51 The difference was that the ‘biggest loser’, the lineage with the lowest relative abundance, was

52 assigned different kinetics. This approach allowed us to relate quantifiable kinetic changes to the
53 likelihood that the failing lineage would overcome drift-driven failure and thrive. We also
54 determined how the required degree of change varied under differing crowding intensities (e.g.,
55 closer spacing and increased initial population size).

56 We found that under purely stochastic conditions the losing lineage varied unpredictably between
57 runs, showing the expected effects of drift. Further, altering kinetics did enable losing lineages to
58 overcome drift. For example, for an initial population of 9 cells evenly spaced 10 diameters apart
59 either K_s or μ_{max} had to improve by at least 10-20% for a 50% chance of thriving. Crowding affected
60 both the improvement needed for a 50% chance of thriving and the ranges over which both drift and
61 fitness influenced success. The strong and sometimes non-linear interactions between terms could
62 not be adequately reproduced using simple linear estimators but could be adequately expressed with
63 a generalized additive model.

64 2 Methods

65 2.1 Agent Based Model

66 The agent-based model employed NUFEB (Newcastle University Frontiers in Engineering
67 Biology),^{9,10} which is based on the LAMMPS⁹ molecular dynamics simulation framework and has
68 successfully been used to model multi-species biofilms,¹⁰ including development and detachment,⁷
69 trade-offs in extracellular polymeric substance production,¹¹ and phototroph-heterotroph metabolic
70 interactions.¹²

71 NUFEB is not lattice based, cells were positioned in three dimensions and had individual dynamic
72 sizes. The directions in which cells divided and biomass allocations (40 to 60%) during division were
73 randomly determined using a Park-Miller pseudorandom number generator and were the two factors
74 contributing to drift.

75 The individually simulated bacterial cells physically interacted using realistic physics and grew
76 according to Monod-style models described by Equation (1) where μ is the substrate-dependent
77 growth rate (1/hr), μ_{max} is the maximum specific growth rate (1/hr), $[S]$ is the concentration of the
78 relevant substrate (kg/m³), and K_s is the half-saturation constant for the substrate (kg/m³). Additional
79 descriptions of NUFEBs mechanics are detailed in previous publications.^{9,10}

$$\mu = \mu_{max} \frac{[S]}{K_s + [S]} \quad (1)$$

80 The simulation volume height (2x10⁻⁴ m) was defined to be in the Z-dimension, the bulk substrate
81 concentration boundary condition at the top of the simulation volume was 1x10⁻⁴ kg/m³ and the
82 initial substrate concentration throughout the volume was set to the same value. The X and Y
83 dimensions were equal and varied based on spacing and number of initial cells. Additionally, the X
84 and Y boundaries were periodic, allowing biomass and substrates to wrap from one side of the
85 simulation to the other.

86 2.1.1 Model Implementation Details

87 NUFEB simulates bacterial growth, physical interactions, and substrate diffusion and reactions
88 within a cuboid volume. Bacterial growth is given as mass over time and determined by a summation
89 of Monod-style rate equations and the change in mass is used to calculate the diameter of a spherical
90 organism. When an individual grows beyond a user-defined threshold (here 1.36 microns), it divides
91 into two organisms. The first cell receives 40-60% of the biomass (uniformly randomly selected) and
92 the second cell receives the remainder. The three-dimensional direction of division relative to the
93 centre of the initial cell is randomly chosen. Mechanically, the individuals are subjected to contact,
94 adhesion, and fluid forces which are implemented as respective as spring and dashpot, spring, and
95 simple one-way coupling physical models. A mechanical relaxation step is performed to address the
96 mechanical in-equilibrium introduced by organism division. With respect to the crowding explored
97 in this research, the result of mechanical relaxation is that a freshly cell which finds itself

98 ‘overlapping’ with existing biomass will be part of a ‘shoving’ match in which all relevant
99 individuals will be pushed into nearby empty space.

100 In this simulation a generic nutrient substrate is modelled and oxygen is non-limiting. The substrate
101 is modelled within the cuboid by solving a standard advection-diffusion-reaction equation. The
102 equation is discretized across and solved for small voxel subsections of the cuboid with a short
103 timestep.

104 The implementation used here does not differ from previous detailed explanations¹⁰ employing the
105 the ODD protocol (Overview, Design concepts, Details), which is a standard for agent-based model
106 description. Specifically, the underlying equations regarding growth, transport, and physical
107 interactions have not been modified and the interested reader is guided specifically to the supporting
108 information of reference 10 for an exhaustive, canonical description.

109 2.2 Experimental Approach

110 The base experimental unit was an agent-based simulation initially seeded with identical bacterial
111 cells with starting diameters of 1×10^{-6} m, K_s of 3.5×10^{-5} kg/m³, μ_{max} of 1 h^{-1} , and yield 0.61 kg
112 biomass per kg substrate consumed. The initial cells (total population 4, 9, or 16) were arranged
113 along evenly spaced (2.5, 5, or 10 cell diameters) $M \times M$ points at the base of the simulation volume.
114 Bacteria were allowed to grow and compete until 20% of the simulation volume consisted of
115 heterotrophic biomass.

116 Each combination of populations sizes and spacings was run 120 times using different seed values to
117 initialize the random number generator and the ‘biggest loser’ from each run was identified (see 2.3).
118 Those simulations were then run again, but with the failed lineage given altered kinetic values (see
119 2.4). The results of the runs were used to determine how the altered kinetics contributed to the
120 probability of transitioning from drift-driven failure to a thriving state (see 2.5) under various
121 crowding intensities.

122 All combinations of the factor levels listed in **Table 1** (1089 combinations) were simulated for each
 123 of the 120 seeds, resulting in a total of 130680 runs. Each run required between 2 to 36 hours to
 124 complete, so the simulations were carried out on a high-performance computing cluster (see 2.6).

125 **Table 1:** Experimental factors and levels

Factor	Values									
Spacing (cell diameters)	2.5	5	10							
Initial Population Size	4	9	16							
% Change in K_s	-50	-40	-30	-20	-10	0	10	20	30	40
% Change in μ_{max}	-50	-40	-30	-20	-10	0	10	20	30	50

126 2.3 Determining Failed Lineages

127 For a system initialized with N bacterial lineages, the total biomass X_t is the sum of the biomass for
 128 each lineage X_i , as expressed by equation(2).

$$X_t = \sum_i^N X_i \quad (2)$$

129 In a system where each initial cell is identical, with no competition, and with no random effects, all
 130 X_i are expected to be equal, thus the expected relevant abundance of any lineage (X_E) is given as:

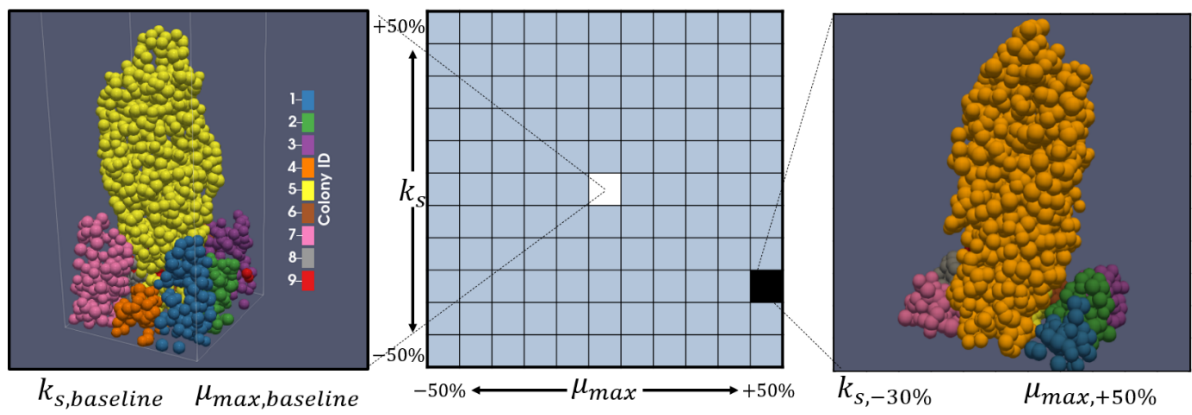
$$X_E = X_t/N \quad (3)$$

131 In the first round of simulations, all initial cells were identical and evenly spaced, but cell division
 132 directions and biomass allocations during division were determined randomly. As a result, the
 133 distribution biomass for any lineage at any particular time was often not equal to the expected
 134 relevant abundance, $X_i \neq X_E$. In practice, there were often one or two lineages which strongly
 135 dominated with $X_i \gg X_E$, one or two lineages which became vanishingly small with $X_i \ll X_E$ (the
 136 ‘biggest losers’), and the rest persisted at some noticeable abundance that was however below X_E .
 137 Moreover, the outcomes appeared to be determined early in the simulation, especially for the best
 138 and worst performing lineages. (Supporting Information Figure S1, Table S1, and Video SV1). We
 139 have defined three classifications of lineage survival based on the difference between X_E and X_i :
 140 *languishing* ($X_i < 0.3 X_E$), *thriving* ($X_i > 0.9 X_E$), and *barely surviving* ($0.3 X_E \leq X_i \leq 0.9 X_E$). The

141 threshold for thriving is lower than XE to accommodate situations where single lineage massively
 142 dominated (e.g., $X_i > 0.6$) leading to lineages which were clearly otherwise doing well but with low
 143 relative abundance.

144 **2.4 Kinetic Alteration for Potential Selective Advantange**

145 The worst-performing bacterial lineages from each of the initial homogenous runs were modified by
 146 altering their individual maximum specific growth rate (μ_{max}) and/or their half-saturation constant
 147 (K_s) (**Figure 1**), potentially giving them a competitive advantage. The altered values were selected as
 148 described in **Table 1**. We acknowledge that not all combinations of μ_{max} and K_s were advantageous
 149 and that μ_{max} and K_s are often strongly correlated; here our goal was to thoroughly explore the
 150 parameter space.



151
 152 **Figure 1:** Illustration of a parameter sweep. Under baseline conditions when all bacteria are identical (left hand side), colony 4 was the
 153 worst performing lineage. When colony 4 was given a potential selective advantage (right hand side) via reduced K_s and increased μ_{max} ,
 154 colony 4 transitioned to thriving. This result along with all other parameter combinations across 120 random seeds was used to
 155 estimate p_{thrive} , the probability that the worst-performing colony would transition to thriving under given altered kinetics. The trend of
 156 upward growth by the bacteria is due to substrate concentration gradients and is characteristic of growth under low-nutrient
 157 conditions.¹⁰

158 A two-dimensional parameter space was chosen because both μ_{max} and K_s met two desirable criteria.
 159 First, they directly associate growth and substrate concentration. Second, they are major parameters
 160 used when designing bioreactors, calibrating associated models, and when discussing kinetic control
 161 of microbial populations within reactors. A composite ratio of the parameters did not appear usable
 162 due to a lack of symmetry in results (e.g., across the upper-left to lower-right diagonals in Figure 4).
 163 The disadvantage of such an approach is the large computational cost. For similar work where those

164 criteria do not apply, a one-dimensional parameter space is suggested. Ideally, this single-parameter
165 would be part of the underlying biological model (such as yield), rather than a generic multiplicative
166 ‘selective advantage’ variable .

167 2.5 Probability Map Generation

168 The kinetic parameter sweeps were used to generate tables for each combination of factors which
169 listed the final relative biomass of each bacterial lineage, that lineage’s status as the ‘biggest loser’,
170 and the lineage’s success under each run. Within each combination population size and spacing, the
171 percentage of failing lineages which transitioned to thriving during the parameter sweep was
172 recorded across all seeds. *s.* Those percentages represent the probabilities that the selective advantage
173 (if any) conferred by altered kinetics would outweigh drift-driven failure under the given conditions.

174 2.6 Simulation Management

175 Simulations were run and their results tabulated on the Newcastle University Rocket High
176 Performance Computing environment and managed using Snakemake^{13,14} workflows populating a
177 SLURM¹⁵ queue. Each simulation was run on a single core, with multiple hundreds of simulations
178 run in parallel. Job submissions encompassed all kinetic parameter sweeps for each combination of
179 other parameters, *e.g.*, a single batch submission would consist of all combinations of μ_{max} and K_s for
180 4 bacteria, spaced 5 diameters apart.

181 2.7 Data Analysis

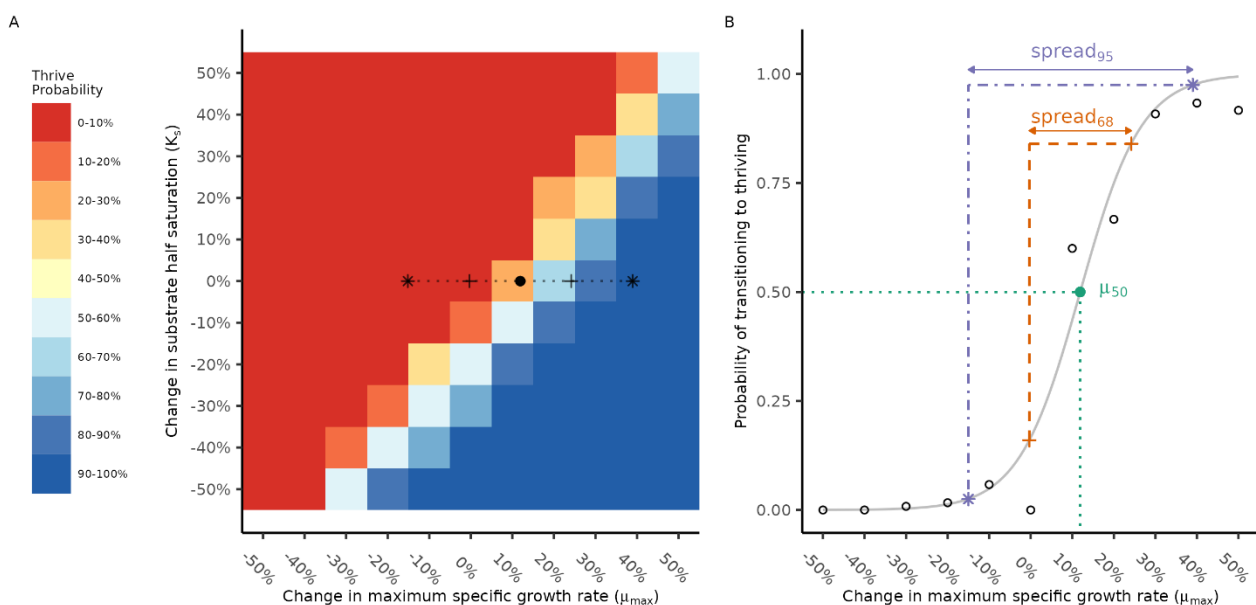
182 Simulation results were saved as tabular comma separated value (CSV) text files and aggregated
183 using BASH¹⁶ (v. 4.2) shell and Python¹⁷ (v. 3.8) scripts which included the NumPy¹⁸ and pandas¹⁹
184 libraries. Further processing of the data was performed off the cluster and used R²⁰ (v. 4.2) scripts
185 incorporating various Tidyverse²¹ and other supporting packages.²²⁻⁴³

186 2.7.1 Parameters Quantifying the Balance Between Drift and Selection

187 Each probability map was conceptually analogous to a cliffside; a continuous sharp probability
 188 threshold gradient separated by two flat regions of either 100% lineage success or failure (**Figure 2**
 189 A). We wished to quantify the midpoint and steepness of the gradient along lines of constant K_s for
 190 each crowding condition. A cross-section of the probabilities along μ_{max} for any constant K_s produces
 191 a sigmoid-shaped profile (**Figure 2 B**). The profiles were fit to a logistic function of μ_{max} with a
 192 maximum value of 1 given by equation (4), where p_{thrive} is the probability of transitioning to a
 193 thriving colony, k is a parameter affecting the steepness of the curve, and μ_{50} is the μ_{max} value at
 194 which there is a 50% probability of thriving.

$$p_{thrive} = \frac{1}{1 + e^{-k*(\mu_{50} - \mu_{max})}} \quad (4)$$

195 The relevant k and μ_{50} parameters from each fit were recorded. We also determined the domains of
 196 μ_{max} values associated with the p_{thrive} ranges covering either a 2.5-97.5% or 16-84% chance of
 197 thriving. These domains, respectively named $spread_{95}$ and $spread_{68}$ quantified the regions over which
 198 both drift and selection influenced success.



199
 200 **Figure 2:** Illustration of how the μ_{50} and $spread$ parameters were calculated. In this example, the probability map corresponding to 4
 201 initial organisms placed 5 diameters apart is shown (A), and the dashed line is drawn along a line of constant K_s . The full length of the
 202 line denotes the $spread_{95}$ region, the portion between crosses denotes $spread_{68}$, and the solid point represents the μ_{50} mark. When the
 203 p_{thrive} values are plotted as a function of μ_{max} along the line of constant K_s , (B) it is apparent that a logistic function (grey solid line)

204 may be fitted to the points (black rings). The fitted function was used to estimate both the value of μ corresponding to μ_{50} and the
205 widths of the *spread* regions. This analysis was repeated for all crowding conditions along all lines of constant K_s .

206 The results of all sigmoid fits are shown in Supporting Information Figures S2-S10.

207 2.7.2 Analysing Balance Parameters

208 Within each crowding scenario, the extracted parameters were analysed using simple linear
209 regression models of the parameters as functions of K_s . The effect of crowding pressure (spacing and
210 total population) was then analysed by comparing the results of the fits between scenarios.

211 We note that although the linear fits for a 2nd order polynomial on μ_{50} generally resulted in
212 marginally improved R^2 scores and removed parabolic patterns from the residuals, the simple linear
213 regressions were still excellent and more interpretable; care should be taken if extending this work to
214 larger ranges of kinetic values.

215 2.7.3 Modelling the Effect of Competitive Pressure and Altered Kinetics

216 We wished to determine if a model based on the simulation results could accurately reproduce the
217 transition probabilities for each crowding scenario. The ultimate goal of these models was not
218 prediction, but to provide a descriptive framework⁴⁴ showing which factors, interactions, and
219 potential non-linearities were important. Variations on both multiple linear regression models (MLR)
220 and Generalized Additive Models (GAMs)⁴⁵ were fitted to either the log-likelihood of p_{thrive} (for
221 MLRs) or directly to p_{thrive} (GAMs).

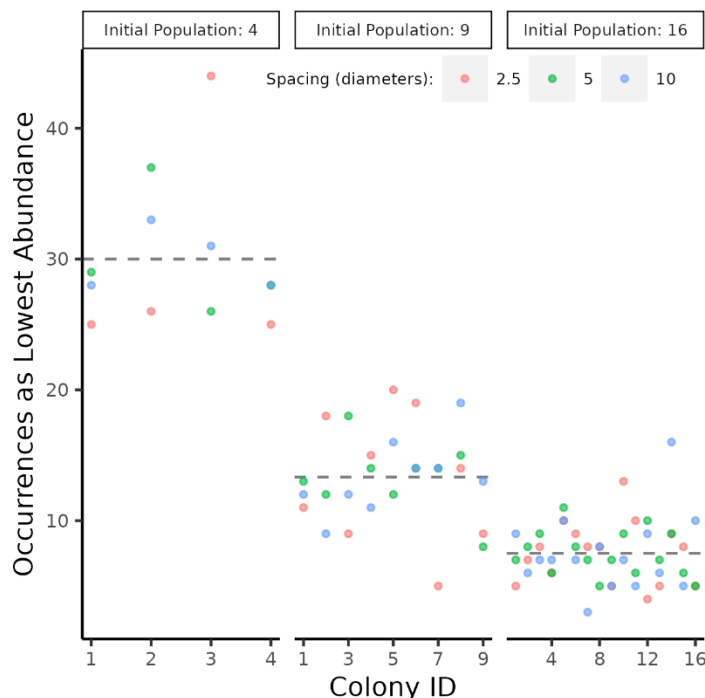
222 In both cases, backward step selection from factorial models incorporating up to three-way
223 interactions was performed to select the final model. Non-significant ($p > 0.05$) terms were
224 iteratively removed from the model starting with the highest order interactions. Main effects were
225 retained even if non-significant when they were part of a significant interaction term.

226 The final models were selected based on R^2 and Akaike Information Criterion (AIC) values as well
227 as interpretability. The potential models and the associated fit criteria are included in Supporting
228 Information Tables S2-S5.

229 3 Results

230 3.1 Drift Occurred When All Cells Were Identical

231 A foundational assumption of this approach is that even in a system with equally spaced, identical
232 microbes, random growth will lead to drift. We tested this assumption for crowding scenarios where
233 all microbes had identical base K_s and μ_{max} parameters by determining the number of times each
234 lineage was the ‘biggest loser’ over 120 simulations (Figure 3) and, similar to testing m dice for
235 fairness, applied a Chi-Square test ($\alpha=0.05/m$) where m is a Bonferroni correction for multiple testing
236 ($m=9$ at 3x3 initial spacings and population sizes). Each initial site was statistically as likely as any
237 other to be the biggest loser (Supporting Information Table S6).



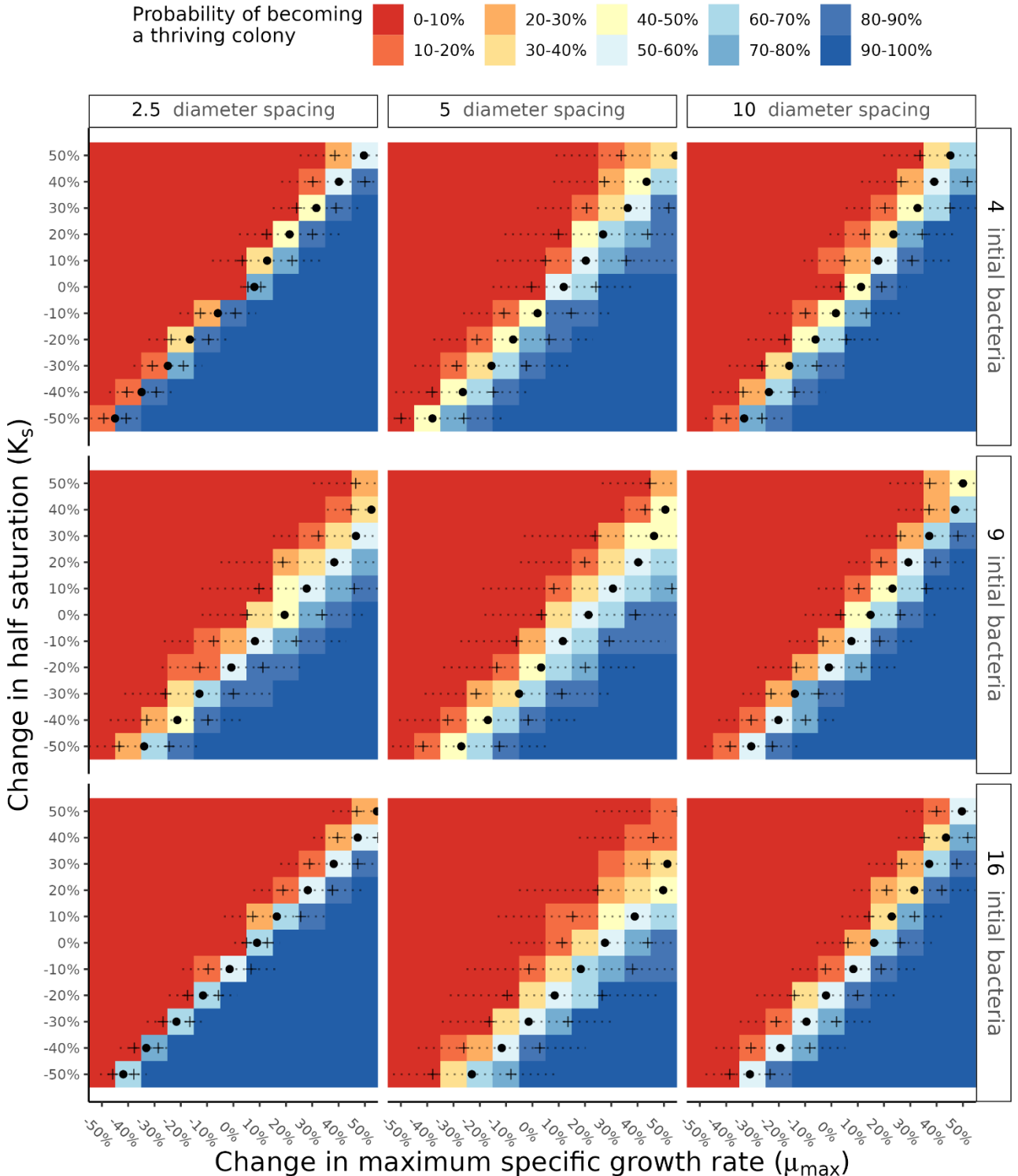
238
239 **Figure 3:** The number of times each colony was the least successful performer during all 120 runs of the baseline simulation where all
240 bacteria were identical. Dashed grey lines indicate the expected value. Points are colored based on spacings between initial sites. For
241 each set of initial populations, no colony appeared biased away from the expected number of failures.

242 Additionally, the relative proportion of lineages which languished, survived, or thrived for each set
243 of crowding conditions was determined. Simulations, on average, had between one and two thriving
244 lineages, with the rest languishing (65-75% for 4 initial sites, 80-88% others), and a few (0-5%)
245 which did not thrive but grew to non-negligible abundance (Supporting Information Table S1). When

246 4 organisms were initially present, only languishing and thriving lineages existed, there was
247 otherwise no clear trend between these ratios and either the number or spacing of initial bacteria.

248 3.2 The Least Successful Lineages Could Overcome Drift with Altered Kinetics

249 As expected, altering the kinetics of an organism could give it a chance to overcome drift-driven
250 failure (**Figure 4**).



251
252 **Figure 4:** Changing the μ_{max} and K_s of the least successful lineage was associated with a probability of transitioning to a thriving
253 status. Solid dots represent μ_{50} , the percent change in μ_{max} at a given K_s associated with 50-50 odds of thriving. Dashed lines show the
254 range of μ_{max} corresponding to a p_{thrive} of 2.5 to 97.5 (i.e., $spread_{95}$). Crosses indicate the analogous $spread_{68}$ region.

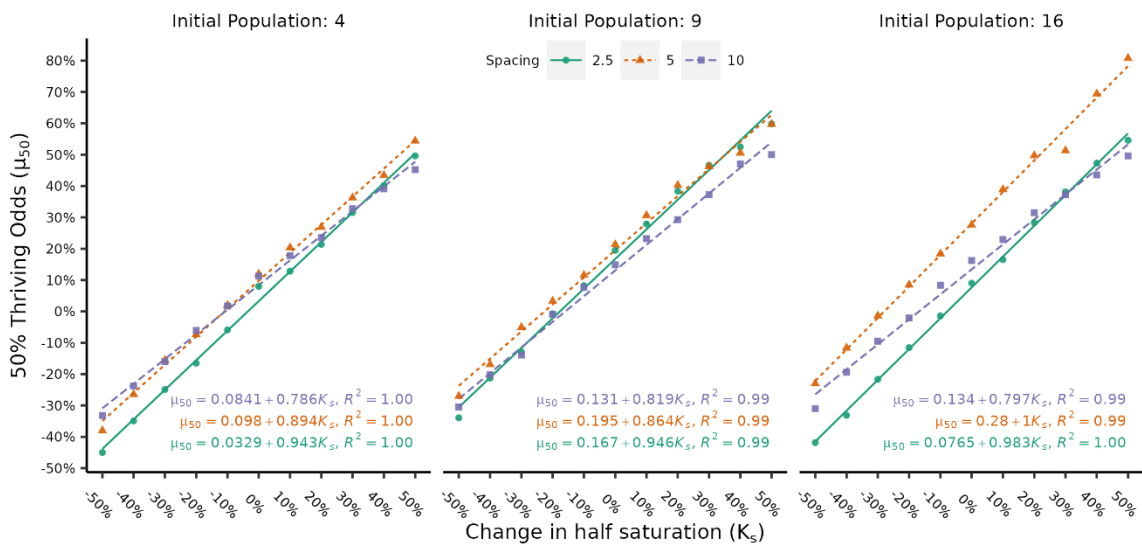
255 The increases in μ_{max} corresponding to the least successful lineage having a 50% chance to become
256 thriving, which we denote as μ_{50} , are represented by the dark circles in **Figure 4**. At the baseline K_s a
257 typical μ_{50} is in the range of 10-30%, with the exact value affected by initial spacing and population

258 size (*i.e.*, crowding). Decreasing K_s , as expected, reduces μ_{50} – even to the point where so long as
259 substrate uptake affinities are ‘good enough’, the initially failing organism may have excellent odds
260 despite having a μ_{max} notably lower than its peers. The overall effect, for a given crowding
261 condition, is a semi-linear ‘cliff’ of μ_{50} values where μ_{50} changes inversely with K_s . Qualitatively
262 speaking, the location of that ‘cliff’ was shifted to the right (higher μ_{50}) when crowding was
263 increased via initial population size or when comparing between the extremes of spacing.
264 Areas where the probability of thriving is neither 0 nor 1, are, by definition, areas where drift and
265 selection both influence success. The widths of these areas are denoted as *spread* and are indicated
266 by the dotted horizontal lines and crosses in **Figure 4**. The full length of the line denotes the $spread_{95}$
267 area, which is the range of μ_{max} for a given K_s which corresponds to a 2.5% to 97.5% chance of
268 thriving. The crosses represent a similar range, $spread_{68}$, which corresponds to a 16% to 85% chance
269 of thriving.
270 Because the μ_{50} values are also the centre point of the *spread* regions, *spread* shifted in the same
271 manner as μ_{50} . However, the actual magnitudes of *spread* did not necessarily follow the same
272 patterns. First, there was no guaranteed symmetry about K_s . For example, for 9 initial organisms
273 separated by 5 diameters, the $spread_{95}$ for K_s of -30% and 30% are visibly different (**Figure 4**, row 2
274 column 2). Though the asymmetry varied between crowding conditions, it generally manifested as
275 *spread* widening with increasing K_s . Second, there was no clear monotonic trend with *spread* values
276 corresponding to crowding. A spacing of 5 diameters appeared to produce the widest spreads,
277 *ceteris paribus*. Further, there was no clear rule determining which of the two spacing extremes
278 would have a larger *spread*. For example, with 4 initial bacteria a spacing of 10 diameters resulted in
279 larger spreads than in 2.5 diameters, but the opposite occurred with 16 initial bacteria.

280 3.3 Quantitative Effect of Crowding on μ_{50} and *spread*

281 The qualitative effects of crowding described in the previous section were quantified via simple
 282 linear regression as described in section 2.7.2.

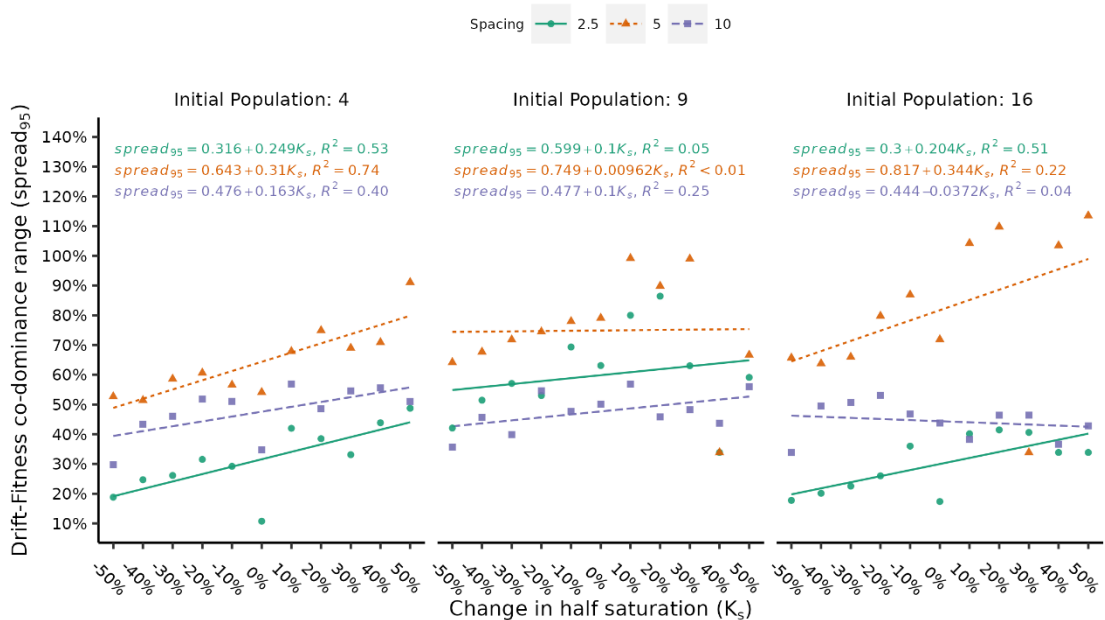
283 For any given crowding condition μ_{50} , the relative change of μ_{max} at which the worst performing
 284 lineage had a 50% chance to transition towards thriving, was essentially linear with respect to K_s and
 285 the correlation coefficient was uniformly high (Figure 5). The slopes of these relationships indicate
 286 the change in μ_{50} required to compensate for a change in K_s . At the tightest spacing, μ_{50} had to
 287 change the most, with a ratio of essentially 1:1 and a slight monotonic increase corresponding to
 288 initial population size. As initial spacings widened, the ratio almost always decreased for any initial
 289 population size. Across initial population sizes, the ratio for 5 and 10 diameter spacings appeared to
 290 follow a general trend of increasing, but this was not monotonic.



291
 292 **Figure 5:** Under each crowding condition, μ_{50} changed linearly with K_s . Large initial population sizes increased the differences
 293 between spacings, moderate spacings generally required the largest absolute μ_{50} , but the tightest spacings required the largest change
 294 μ_{50} in per unit change in K_s .

295 The absolute value of μ_{50} was strongly affected by differences between the fitted intercepts. For
 296 example, a 2.5 diameter spacing under an initial population size of 16 had a high slope (0.983) but
 297 also the lowest required μ_{50} of all spacings under the same conditions until a 30% change in K_s . The
 298 practical difference between spacing was largest at high initial population size, indicating a potential
 299 interaction between these factors.

300 Unlike μ_{50} , the range over which both drift and selection effects influenced success, $spread_{95}$ did not
 301 have a simple linear relationship with K_s , with many poor R^2 values, residual patterns, and high
 302 leverage datapoints (Figure 6). There was also no clear, consistent relationship applicable across
 303 factors. In general, linear fits became worse with increasing population size which appeared to
 304 produce higher variance and generated more high-leverage points, especially at separation distances
 305 of 5 diameters. These issues were largely the same when the analysis was repeated for $spread_{68}$
 306 (Supporting Information Figure S13). There is little to concretely say except that the $spread$ was
 307 most often widest at moderate spacings, generally increased with K_s , and had a noisy, complicated
 308 relationship with initial population size and spacing.



309
 310 **Figure 6:** Under each crowding condition, $spread_{95}$ changed with K_s . Insofar as trends were present, moderate spacing produced the
 311 widest $spread_{95}$ and the differences between spacings increased with population size.

312 3.4 Description via Multiple Linear Regression and Generalized Additive Models

313 The simulation results were modelled using both multiple linear regression (MLR) and a generalized
 314 additive model(GAM) respectively described by equations (5) and (6) where: p_{thrive} is the probability
 315 of transitioning to a thriving status, μ_p and K_p are the respective percent changes from the baseline
 316 μ_{max} and K_s , N_0 is the initial population size, s_i is the initial spacing (in diameters) between
 317 organisms, and ε is a small pseudo-probability (1×10^{-6}) added to avoid division by 0 and issues with

318 log transformation. For linear terms in equations (5) and (6), β_i denotes the fitted coefficient for term
 319 i with $i=0$ representing the intercept. Terms to which GAM smoothing was applied are represented
 320 by $s(\dots)$ in equation (6) with interactions between a smoothed variable x and linear variable y
 321 denoted as $s(x, \text{by } y)$. Significant terms ($p < 0.05$) are highlighted in bold. The associated
 322 coefficients, significance values, and other relevant fitting information are included in Supporting
 323 Information Tables S2-S5.

$$\log\left(\frac{\mathbf{p}_{thrive}}{1 - \mathbf{p}_{thrive} + \varepsilon}\right) = \boldsymbol{\beta}_0 + \boldsymbol{\beta}_1 \mu_p + \boldsymbol{\beta}_2 K_p + \boldsymbol{\beta}_3 N_0 + \boldsymbol{\beta}_4 s_i + \boldsymbol{\beta}_5 \mu_p s_i + \boldsymbol{\beta}_6 K_p s_i \quad (5)$$

$$\begin{aligned} p_{thrive} = & \beta_0 + s(\mu_p) + s(K_p) + s(N_0) + s(s_i) + s(\boldsymbol{\mu}_p K_p) + s(\boldsymbol{\mu}_p s_i) + s(K_p s_i) \\ & + s(N_0, \text{by } s_i) + s(\boldsymbol{\mu}_p K_p N_0) + s(\boldsymbol{\mu}_p K_p s_i) \end{aligned} \quad (6)$$

324 The MLR model captured the general behaviour of the shift in the boundary between low and high
 325 thriving probabilities but did not adequately reproduce changes in *spread* (**Figure 7 A vs. C**). The
 326 overall root-mean-squared error (RMSE) of the model was 0.125. While most predicted probabilities
 327 differed from the simulation by no more than ± 0.1 , some predictions were subject to large error
 328 (**Figure 7 A, D, F** and Supporting Information Figures S11 and S14-S15). The largest errors
 329 unsurprisingly appear closest to the boundary between low and high p_{thrive} regions with the MLR
 330 model over-optimistic at the extremes of spacing and lower initial population size. Conversely, the
 331 model tended towards overly pessimistic at moderate spacing.

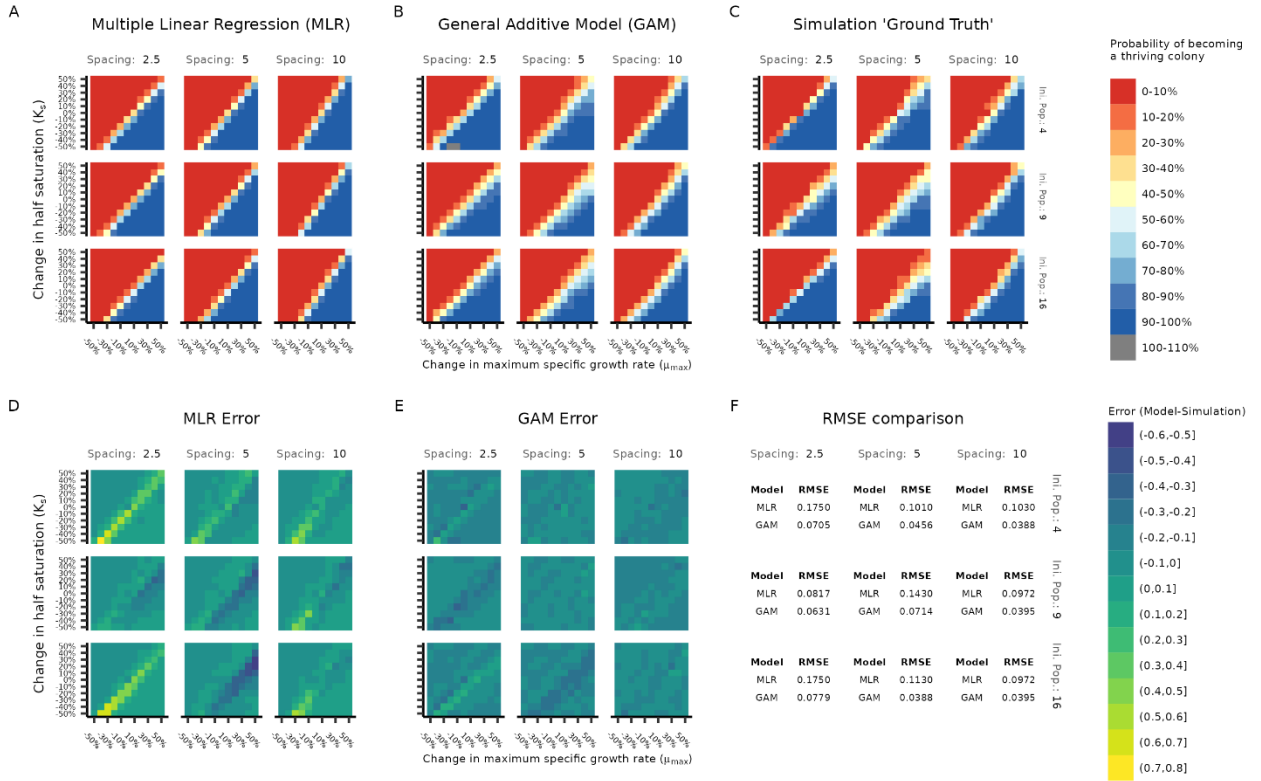


Figure 7: Predictions of MLR model (A) and GAM (B). Simulation results in (C) are presented for ease of comparison. The model errors for the MLR (D) and GAM (E) are presented visually as well as quantified per-crowding condition in (F). The GAM outperformed the MLR, which particularly failed to capture *spread*, was overly optimistic at spacing extremes, and pessimistic at moderate spacing. The small region of greater than 100% odds occurred because the GAM was not constrained to predicting values in the range of [0,1]. Larger individual plots of panels A, B, D, and E are available in Supporting Information figures S14-S17.

332
333
334
335
336
337

338 In comparison to the MLR model, the GAM not only captured the general boundary shift but also the
339 changes in *spread* (Figure 7 B vs. C in contrast to A vs. C). The overall RMSE of the GAM was
340 0.0563, or somewhat better than half the RMSE of the MLR model. As with the MLR model, most
341 predicted probabilities differed from the simulation by no more than ± 0.1 . Unlike the MLR model,
342 there were fewer exceptionally large errors and those which did occur were of smaller magnitude
343 (Figure 7 B, E, F and Figures S12 and S16-S17). The GAM followed the same trends in over- and
344 under-prediction as the MLR.

345 **4 Discussion**

346 **4.1 Crowding Affects the Balance Between Drift and Selection**

347 The two parameters describing the balance between drift and selection, μ_{50} and *spread*, were both
348 affected as crowding became more intense due to either decreased initial spacing or increased initial

349 population size. It was originally expected that as crowding intensity increased, greater selective
350 advantages would be required (μ_{50}) along with a decrease in the range of values over which both drift
351 and selection influenced success (*spread*). That was not the case.

352 Instead, the largest *spread* values predominately occurred at moderate (5 diameter) initial spacing.
353 We suggest the cause is physical competition for space, specifically the practical significance of
354 single 'bad' random choices in division direction and biomass allocation. When bunched tightly
355 together, competition for space is intense and even a few poor random events can consign a lineage
356 to languishing despite a moderate growth advantage. At the other extreme, spatial competition is
357 lessened sufficiently that a few missteps do not guarantee ruin, allowing a lineage to take the full
358 benefit of any growth advantage. Meanwhile, at moderate spacing, immediate neighbours are close
359 enough so that poor random events are harmful but not necessarily disastrous and, at the same time,
360 growth advantages are somewhat hindered, but still helpful. Remembering that *spread* quantifies the
361 region where both fitness and drift influenced success, it then makes sense that we observed the
362 largest *spread* values at moderate spacing.

363 The 50-50 odds point, μ_{50} , was also slightly larger at moderate spacings, although not consistently
364 and the effect size was not practically different except at large population sizes. The underlying basis
365 for why is not entirely clear, numerically it was due to the consistently larger intercept (Figure 5).
366 The trend of the slopes is, however, more easily explained and we attribute it to competition for
367 substrate. For any initial population size, smaller spacings resulted in higher slopes. In other words,
368 to maintain the 50-50 odds when K_s was poor, μ_{50} had to change more at closer spacing. This makes
369 intuitive sense – closer spacings result in lower local substrate concentrations, and any deficit to K_s is
370 more deleterious to selection.

371 Increased initial population sizes had more straightforward, secondary, effects on μ_{50} and K_s . As the
372 initial population size increased, the differences between spacings became more pronounced, but the

373 general trends remained unchanged. In other words, more competitors are problematic, especially as
374 it relates to diffusible substrate, but the major influence on success is competition for space between
375 immediate neighbours.

376 4.2 Interactions Between Factors Incorporating Non-Linear Effects are Important

377 In the MLR a main-effects only model (RMSE 0.125, R^2 of 0.820) performed essentially identically
378 to the MLR model with interactions (RMSE 0.127, and R^2 of 0.820), however neither adequately
379 reproduced simulation results. Both were especially poor at representing the regions where fitness
380 and drift influenced success. A GAM which incorporated only main effects using non-linear
381 smoothing quantitatively performed slightly worse than either MLR main-effects model (RMSE
382 0.197 and R^2 of 78.1), but drastically and uniformly overpredicted spread. Only when both
383 interactions and smoothing were incorporated did a model adequately reproduce the simulation
384 results (Figure 7 and Supporting Information Figure S17). It is visually apparent in the simulation
385 results and quantified in the fitting results (Supporting Information Table S4-5) that interactions are
386 important, particularly those involving spacing. Further, the non-linearity of the interactions
387 (measured as the departure of the term's extended degrees of freedom from a value of 1), is
388 particularly high for any interaction incorporating both μ_p and K_p and less so but still notably for
389 interactions incorporating spacing (Supporting Information Table S5).

390 4.3 Limitations and Extensions

391 The simulated conditions were deliberately chosen to isolate the effect of drift. While this made the
392 work tractable, a system wherein every organism is completely identical, starts growing at the same
393 time, and is initially evenly spaced on a grid does not frequently occur in nature. Although we
394 believe the general themes uncovered translate to real ecological systems, the exact quantification
395 does not and is not mean to apply to all situations. Future work should focus on stochastically placed
396 (in time and space) populations with natural variability in Monod parameters.

397 Extending the work so that the simulated community reflects a more natural distribution would also
398 enable validation of the model, as, despite promising advances,⁴⁶ it is currently infeasible to exactly
399 place essentially identical bacteria at the resolution required.

400 Additional parameters affecting drift and selection should also be evaluated – especially the
401 influence of nutrient-rich conditions⁴⁷ and how a change to yield, rather than growth rate, alters
402 success.⁴⁸ Adding these factors requires however overcoming the curse of dimensionality, the current
403 simulations took over 1 year of real-world time and 175 years' worth of CPU time. Given the large
404 areas where 'nothing interesting' happens, designing further experiments to incorporate adaptive
405 sampling⁴⁹ is a promising solution. Further, adaptive sampling would enable, at the same
406 computational cost, exploring a larger range of μ_{max} and K_S variation (which may vary by orders of
407 magnitude in real-world conditions⁵⁰) and at a greater degree of resolution than 10% changes in the
408 region where the probabilities rapidly change.

409 5 Conclusion And Relevance to Real World Systems

410 It is apparent that during biofilm formation in low nutrient conditions, drift strongly determines
411 which organisms thrive and which organisms fail, so long as they have similar growth rates and
412 substrate affinities. Even when those parameters differ between individuals by $\pm 50\%$, there are still
413 large regions where a selective advantage does not guarantee overcoming drift-driven failure.
414 In fact, we observed the lineage fates were determined very early in the simulations and for these
415 systems 'well-begun is half done'. We speculate that this may be a piece to the puzzle explaining the
416 apparent contradiction between actual and effective community size in neutral modelling⁴ – the
417 bacteria are not in competition with the full steady-state community but only the immediate smaller,
418 community near the beginning of biofilm growth. However, the conditions studied here violate the
419 steady state assumption of that work, so a more careful analysis is warranted.

420 The conditions we have described are not dissimilar from those within an aerated portion of a
421 wastewater treatment plant, where tightly packed bacterial aggregates are suspended in a bulk liquid
422 and where substrate concentrations are often quite low, especially during operation as a completely
423 mixed stirred reactor (albeit somewhat higher than simulated here). Further, these bacteria are
424 recirculated through the system and relatively well-adapted to domestic wastewater, thus already
425 selected for similarity. Based on the results presented here, we would expect to see a system in which
426 there is a high degree of random turnover in organism identity, but relatively stable functional and
427 biological activity, which is exactly what has been observed in wastewater treatment plants.^{51,52}

428 6 Acknowledgements

429 We wish to acknowledge the United States National Science Foundation Directorate for Biological
430 Sciences for funding via the Postdoctoral Research Fellowships in Biology (NSF PRFB Award #
431 2007151) and the Newcastle University Rocket HPC computing cluster. We also thank Tom Curtis
432 for his valuable feedback and encouragement, Denis Taniguchi and Bowen Li for their help in
433 understanding the NUFEB software, and countless helpful comments from many interested parties
434 during poster sessions and talks.

435 7 Competing Interests

436 The author has no competing interests.

437 8 Data Availability Statement

438 The data analysis code, data from the simulations, and exact NUFEB variant are respectively located
439 in the following repositories:
440
441 Analysis: https://github.com/joeweaver/agent_based_biofilm_drift/
442 Data: <https://osf.io/fch3z/>
443 NUFEB variant: https://github.com/nufeb/NUFEB-dev/tree/compute_vol_group

444 9 References

445 (1) Vellend, M. Conceptual Synthesis in Community Ecology. *The Quarterly Review of Biology*
446 **2010**, *85* (2), 183–206. <https://doi.org/10.1086/652373>.

447 (2) Battin, T. J.; Sloan, W. T.; Kjelleberg, S.; Daims, H.; Head, I. M.; Curtis, T. P.; Eberl, L.
448 Microbial Landscapes: New Paths to Biofilm Research. *Nat Rev Microbiol* **2007**, *5* (1), 76–81.
449 <https://doi.org/10.1038/nrmicro1556>.

450 (3) Nemergut, D. R.; Schmidt, S. K.; Fukami, T.; O'Neill, S. P.; Bilinski, T. M.; Stanish, L. F.;
451 Knelman, J. E.; Darcy, J. L.; Lynch, R. C.; Wickey, P.; Ferrenberg, S. Patterns and Processes of
452 Microbial Community Assembly. *Microbiol Mol Biol Rev* **2013**, *77* (3), 342–356.
453 <https://doi.org/10.1128/MMBR.00051-12>.

454 (4) Sloan, W. T.; Nnaji, C. F.; Lunn, M.; Curtis, T. P.; Colloms, S. D.; Couto, J. M.; Pinto, A. J.;
455 Connelly, S.; Rosser, S. J. Drift Dynamics in Microbial Communities and the Effective
456 Community Size. *ENVIRONMENTAL MICROBIOLOGY* **2021**, *23* (5), 2473–2483.
457 <https://doi.org/10.1111/1462-2920.15453>.

458 (5) Zhou, J.; Liu, W.; Deng, Y.; Jiang, Y.-H.; Xue, K.; He, Z.; Van Nostrand, J. D.; Wu, L.; Yang,
459 Y.; Wang, A. Stochastic Assembly Leads to Alternative Communities with Distinct Functions in
460 a Bioreactor Microbial Community. *MBIO* **2013**, *4* (2). <https://doi.org/10.1128/mBio.00584-12>.

461 (6) Dini-Andreote, F.; Stegen, J. C.; van Elsas, J. D.; Salles, J. F. Disentangling Mechanisms That
462 Mediate the Balance between Stochastic and Deterministic Processes in Microbial Succession.
463 *Proceedings of the National Academy of Sciences* **2015**, *112* (11), E1326–E1332.
464 <https://doi.org/10.1073/pnas.1414261112>.

465 (7) Cira, N. J.; Pearce, M. T.; Quake, S. R. Neutral and Selective Dynamics in a Synthetic Microbial
466 Community. *Proc. Natl. Acad. Sci. U.S.A.* **2018**, *115* (42).
467 <https://doi.org/10.1073/pnas.1808118115>.

468 (8) Fodelianakis, S.; Valenzuela-Cuevas, A.; Barozzi, A.; Daffonchio, D. Direct Quantification of
469 Ecological Drift at the Population Level in Synthetic Bacterial Communities. *ISME JOURNAL*
470 **2021**, *15* (1), 55–66. <https://doi.org/10.1038/s41396-020-00754-4>.

471 (9) Li, B.; Taniguchi, D.; Gedara, J. P.; Gogulancea, V.; Gonzalez-Cabaleiro, R.; Chen, J.;
472 McGough, A. S.; Ofiteru, I. D.; Curtis, T. P.; Zuliani, P. NuFeb: A Massively Parallel Simulator
473 for Individual-Based Modelling of Microbial Communities. *PLoS Computational Biology* **2019**,
474 *15* (12), e1007125. <https://doi.org/10.1371/journal.pcbi.1007125>.

475 (10) Jayathilake, P. G.; Gupta, P.; Li, B.; Madsen, C.; Oyebamiji, O.; González-Cabaleiro, R.;
476 Rushton, S.; Bridgens, B.; Swailes, D.; Allen, B.; McGough, A. S.; Zuliani, P.; Ofiteru, I. D.;
477 Wilkinson, D.; Chen, J.; Curtis, T. A Mechanistic Individual-Based Model of Microbial
478 Communities. *PLoS ONE* **2017**, *12* (8), e0181965. <https://doi.org/10.1371/journal.pone.0181965>.

479 (11) Jayathilake, P. G.; Jana, S.; Rushton, S.; Swailes, D.; Bridgens, B.; Curtis, T.; Chen, J.
480 Extracellular Polymeric Substance Production and Aggregated Bacteria Colonization Influence
481 the Competition of Microbes in Biofilms. *FRONTIERS IN MICROBIOLOGY* **2017**, *8*.
482 <https://doi.org/10.3389/fmicb.2017.01865>.

483 (12) Sakkos, J. K.; Santos-Merino, M.; Kokarakis, E. J.; Li, B.; Fuentes-Cabrera, M.; Zuliani, P.;
484 Ducat, D. C. Predicting Partner Fitness Based on Spatial Structuring in a Light-Driven Microbial
485 Community. *bioRxiv* September 30, 2022, p 2022.09.28.510001.
486 <https://doi.org/10.1101/2022.09.28.510001>.

487 (13) Mölder, F.; Jablonski, K. P.; Letcher, B.; Hall, M. B.; Tomkins-Tinch, C. H.; Sochat, V.;
488 Forster, J.; Lee, S.; Twardziok, S. O.; Kanitz, A.; Wilm, A.; Holtgrewe, M.; Rahmann, S.;
489 Nahnsen, S.; Köster, J. Sustainable Data Analysis with Snakemake. *F1000Research* April 19,
490 2021. <https://doi.org/10.12688/f1000research.29032.2>.

491 (14) Köster, J.; Rahmann, S. Snakemake—a Scalable Bioinformatics Workflow Engine.
492 *Bioinformatics* **2012**, *28* (19), 2520–2522. <https://doi.org/10.1093/bioinformatics/bts480>.

493 (15) Jette, M.; Yoo, A.; Grondona, M. SLURM: Simple Linux Utility for Resource Management;
494 2003. https://doi.org/10.1007/10968987_3.

495 (16) Ramey, C. Bash, the Bourne- Again Shell. In *Proceedings of The Romanian Open Systems*
496 *Conference & Exhibition (ROSE 1994)*, The Romanian UNIX User’s Group (GURU); 1994; pp
497 3–5.

498 (17) Van Rossum, G.; Drake, F. L. *Python 3 Reference Manual*; CreateSpace: Scotts Valley, CA,
499 2009.

500 (18) Harris, C. R.; Millman, K. J.; Walt, S. J. van der; Gommers, R.; Virtanen, P.; Cournapeau,
501 D.; Wieser, E.; Taylor, J.; Berg, S.; Smith, N. J.; Kern, R.; Picus, M.; Hoyer, S.; Kerkwijk, M. H.
502 van; Brett, M.; Haldane, A.; Río, J. F. del; Wiebe, M.; Peterson, P.; Gérard-Marchant, P.;
503 Sheppard, K.; Reddy, T.; Weckesser, W.; Abbasi, H.; Gohlke, C.; Oliphant, T. E. Array
504 Programming with NumPy. *Nature* **2020**, *585* (7825), 357–362. <https://doi.org/10.1038/s41586-020-2649-2>.

505 (19) McKinney, W. Data Structures for Statistical Computing in Python. In *Proceedings of the 9th*
506 *Python in Science Conference*; Walt, S. van der, Millman, J., Eds.; 2010; pp 56–61.
507 <https://doi.org/10.25080/Majora-92bf1922-00a>.

508 (20) R Core Team. *R: A Language and Environment for Statistical Computing*; R Foundation for
509 Statistical Computing: Vienna, Austria, 2022.

510 (21) Wickham, H.; Averick, M.; Bryan, J.; Chang, W.; McGowan, L. D.; François, R.;
511 Grolemund, G.; Hayes, A.; Henry, L.; Hester, J.; Kuhn, M.; Pedersen, T. L.; Miller, E.; Bache, S.
512 Müller, K.; Ooms, J.; Robinson, D.; Seidel, D. P.; Spinu, V.; Takahashi, K.; Vaughan, D.;
513 Wilke, C.; Woo, K.; Yutani, H. Welcome to the Tidyverse. *Journal of Open Source Software*
514 **2019**, *4* (43), 1686. <https://doi.org/10.21105/joss.01686>.

515 (22) Aphalo, P. J. *Ggpmisc: Miscellaneous Extensions to “Ggplot2”*; 2022.

516 (23) Aphalo, P. J. *Ggpp: Grammar Extensions to “Ggplot2”*; 2022.

517 (24) Brand, T. van den. *Ggh4x: Hacks for “Ggplot2”*; 2022.

518 (25) Coretta, S. *Tidymv: Tidy Model Visualisation for Generalised Additive Models*; 2022.

519 (26) Darócz, G. *Logger: A Lightweight, Modern and Flexible Logging Utility*; 2021.

520 (27) Garnier; Simon; Ross; Noam; Rudis; Robert; Camargo; Pedro, A.; Scaini; Marco; Scherer;
521 Cédric. *Viridis - Colorblind-Friendly Color Maps for R*; 2021.
522 <https://doi.org/10.5281/zenodo.4679424>.

523 (28) Henry, L.; Wickham, H. *Purrr: Functional Programming Tools*; 2020.

524 (29) Iannone, R.; Cheng, J.; Schloerke, B. *Gt: Easily Create Presentation-Ready Display Tables*;
525 2022.

526 (30) Kassambara, A. *Ggpubr: “ggplot2” Based Publication Ready Plots*; 2020.

527 (31) Meschiari, S. *Latex2exp: Use LaTeX Expressions in Plots*; 2022.

528 (32) Müller, K. *Here: A Simpler Way to Find Your Files*; 2020.

529 (33) Neuwirth, E. *RColorBrewer: ColorBrewer Palettes*; 2022.

530 (34) Pedersen, T. L. *Patchwork: The Composer of Plots*; 2020.

531 (35) Rij, J. van; Wieling, M.; Baayen, R. H.; Rijn, H. van. Itsadug: Interpreting Time Series and
532 Autocorrelated Data Using GAMMs, 2022.

533 (36) Wickham, H. *Ggplot2: Elegant Graphics for Data Analysis*; Springer-Verlag New York,
534 2016.

535 (37) Wilke, C. O. *Cowplot: Streamlined Plot Theme and Plot Annotations for “Ggplot2”*; 2020.

536 (38) Wilke, C. O. *Ggtext: Improved Text Rendering Support for “Ggplot2”*; 2020.

537 (39) Wolen, A. R.; Hartgerink, C. H. J.; Hafen, R.; Richards, B. G.; Soderberg, C. K.; York, T. P.
538 Osfr: An R Interface to the Open Science Framework. *Journal of Open Source Software* **2020**, *5*
539 (46), 2071. <https://doi.org/10.21105/joss.02071>.

540

541 (40) Wood, S. N. Fast Stable Restricted Maximum Likelihood and Marginal Likelihood
542 Estimation of Semiparametric Generalized Linear Models. *Journal of the Royal Statistical
543 Society: Series B (Statistical Methodology)* **2011**, 73 (1), 3–36.

544 (41) Pedersen, T. L.; Robinson, D. *Gganimate: A Grammar of Animated Graphics*; 2022.

545 (42) Pedersen, T. L. *Transformr: Polygon and Path Transformations*; 2022.

546 (43) Ooms, J. *Gifski: Highest Quality GIF Encoder*; 2022.

547 (44) Caswell, H. The Validation Problem. *Systems analysis and simulation in ecology* **1976**, 4,
548 313–325.

549 (45) Hastie, T.; Tibshirani, R. Generalized Additive Models: Some Applications. *Journal of the
550 American Statistical Association* **1987**, 82 (398), 371–386.
551 <https://doi.org/10.1080/01621459.1987.10478440>.

552 (46) Krishna Kumar, R.; Meiller-Legrand, T. A.; Alcinesio, A.; Gonzalez, D.; Mavridou, D. A. I.;
553 Meacock, O. J.; Smith, W. P. J.; Zhou, L.; Kim, W.; Pulcu, G. S.; Bayley, H.; Foster, K. R.
554 Droplet Printing Reveals the Importance of Micron-Scale Structure for Bacterial Ecology. *Nat
555 Commun* **2021**, 12 (1), 857. <https://doi.org/10.1038/s41467-021-20996-w>.

556 (47) Nadell, C. D.; Foster, K. R.; Xavier, J. B. Emergence of Spatial Structure in Cell Groups and
557 the Evolution of Cooperation. *PLOS Computational Biology* **2010**, 6 (3), e1000716.
558 <https://doi.org/10.1371/journal.pcbi.1000716>.

559 (48) Kretzschmar, J.-U.; Bonhoeffer, S. 2005. The Evolution of Groups of Cooperating Bacteria and the
560 Growth Rate versus Yield Trade-Off. *Microbiology* **151** (3), 637–641.
561 <https://doi.org/10.1099/mic.0.27415-0>.

562 (49) Westermann, P. W.; Evans, R. Adaptive Sampling For Building Simulation Surrogate Model
563 Derivation Using The LOLA-Voronoi Algorithm; Rome, Italy; pp 1559–1563.
564 <https://doi.org/10.26868/25222708.2019.211232>.

565 (50) Cox, C. D. Statistical Distributions of Uncertainty and Variability in Activated Sludge Model
566 Parameters. *Water Environ Res* **2004**, 76 (7), 2672–2685. [https://doi.org/10.1002/j.1554-7531.2004.tb00229.x](https://doi.org/10.1002/j.1554-
567 7531.2004.tb00229.x).

568 (51) Weaver, J. E. *From Floc to Reactor Scales: A Multi-Faceted Investigation Integrating
569 Microbial Ecological Experiments and Computational Modeling to Understand Aerobic
570 Wastewater Systems*; North Carolina State University, 2021.

571 (52) Wang, X.; Wen, X.; Criddle, C.; Yan, H.; Zhang, Y.; Ding, K. Bacterial Community
572 Dynamics in Two Full-Scale Wastewater Treatment Systems with Functional Stability. *Journal
573 of Applied Microbiology* **2010**, 109 (4), 1218–1226. [https://doi.org/10.1111/j.1365-2672.2010.04742.x](https://doi.org/10.1111/j.1365-
574 2672.2010.04742.x).

575